

Stacking-Dependent Van Hove Singularity Shifts in Three-Dimensional Charge Density Waves of Kagome Metals AV_3Sb_5 ($A = K, Rb, Cs$)

Chanchal K. Barman^{a,1}, Sun-Woo Kim^{b,1}, Youngkuk Kim^{a,*}

^aDepartment of Physics, Sungkyunkwan University, Suwon 16419, Korea

^bDepartment of Materials Science and Metallurgy, University of Cambridge, 27 Charles Babbage Road, Cambridge, United Kingdom

Abstract

Vanadium-based kagomé systems AV_3Sb_5 ($A = K, Rb, Cs$) have emerged as paradigmatic examples exhibiting unconventional charge density waves (CDWs) and superconductivity linked to van Hove singularities (VHSs). Despite extensive studies, the three-dimensional (3D) nature of CDW states in these systems remains elusive. This study employs first-principles density functional theory and a tight-binding model to investigate the stacking-dependent electronic structures of 3D CDWs in AV_3Sb_5 , emphasizing the significant role of interlayer coupling in behaviors of the VHSs associated with diverse 3D CDW orders. We develop a minimal 3D tight-binding model and present a detailed analysis of band structures and density of states for various 3D CDW stacking configurations, including those with and without a π -phase shift stacking of the inverse star of David, as well as alternating stacking of the inverse star of David and the star of David. We find that VHSs exist below the Fermi level even in 3D CDWs without π -phase shift stackings, and that these VHSs shift downward in the π -phase shift stacking CDW structure, stabilizing the $2 \times 2 \times 2$ π -shifted inverse star of David distortions in alternating vanadium layers as the ground state 3D CDW order of AV_3Sb_5 . Our work provides the electronic origin of 3D CDW orders, paving the way for a deeper understanding of CDWs and superconductivity in AV_3Sb_5 kagomé metals.

1. Introduction

A kagomé lattice refers to a two-dimensional network of corner-sharing triangles. It offers a fertile ground for studying the intricate interplay between frustrated geometry, topology, and electronic correlations. The electronic energy band structure of a kagomé lattice generically features a flat band, VHSs, and a pair of Dirac points. Depending on the electron filling, various captivating quantum phenomena have been explored, such as quantum topology and geometry [1, 2, 3], superconductivity [4, 5, 6, 7], and quantum magnets [8, 9, 10, 11, 12]. The kagomé lattice in stable materials has been a target of rigorous research efforts, resulting in many experimentally verified materials. Notable examples include FeSn [13], Fe₃Sn₂ [14], and CoSn [15], which illustrates physics originating from flatbands. More recently, kagomé metals such as AV_3Sb_5 [16, 17, 18] and ATi_3Bi_5 [19, 20, 21] for $A = K, Rb, Cs$ and RV_6Sn_6 [22, 23, 24] ($R =$ rare earth), and FeGe [25, 26, 27], have been under intensive investigation to study phenomena associated with the VHSs.

The vanadium-based kagomé metal AV_3Sb_5 ($A = Cs, K, Rb$) has become a prototypical system within the family of kagomé metals. It hosts multiple VHSs near Fermi level that exhibit rich properties [28, 29, 30, 31],

and these VHSs have been found to play a significant role in driving unconventional phenomena [32, 33]. Notably, the onset of an anomalous Hall effect [34, 35] occurs concurrently with the CDW phase transition below $T_{CDW} \approx 80 - 100$ K [17, 36, 37, 38]. The presence of Hall conductivity signals the time-reversal symmetry breaking [39, 40, 41, 42], which is further evidenced by various experiment methods [43, 44, 45]. Moreover, six-fold rotation symmetry breaking at T_{CDW} is observed [46, 47, 48, 49, 50, 51, 52, 53, 54], followed by additional rotational symmetry breaking at lower temperatures [55, 56], which is assigned as electronic nematicity [45, 54, 55]. Upon further cooling, superconductivity emerges with a critical temperature $T_c \sim 0.9 - 2.5$ K [17, 36, 37] and the superconductivity is found to compete with CDW [52, 57, 58, 59].

Despite extensive studies [42, 60, 61, 62, 63, 64, 65, 66], the underlying mechanism of the CDW state, particularly its 3D nature, is not fully understood. It has been well established that the in-plane CDW pattern is either 2×2 star of David (SD) or inverse star of David (ISD) type distortion in the single vanadium kagomé layer [29, 60, 67]. The CDW state in AV_3Sb_5 exhibits a 3D nature with a modulation along the c (out-of-plane) axis. Moreover, CsV_3Sb_5 is also found to exhibit a CDW state with a $2 \times 2 \times 4$ periodicity under certain conditions [67, 68, 69, 70], distinguishing it from KV_3Sb_5 and RbV_3Sb_5 . The energetics of VHSs responsible for the emergence of 3D CDW can provide insight into these phenomena, as the presence of

*Corresponding author

Email address: youngkuk@skku.edu (Youngkuk Kim)

¹These authors contributed equally to this work.

Table 1: TB parameters for AV_3Sb_5 (in eV). ε is the onsite energy. t and t_2 are the nearest-neighbor (NN) and next-nearest-neighbor (NNN) hopping parameters in the kagomé plane [Fig. 1(c)]. t_s is the strength of the CDW order parameter [Figs. 1(d) and 1(e)]. t_{z1} , t_{z2} , t_{z3} , and t_{z4} are NN, NNN, NNNN, and NNNNN hopping strengths along the out-of-plane direction [Fig. 1(f)].

	ε	t	t_2	t_s	t_{z1}	t_{z2}	t_{z3}	t_{z4}
KV_3Sb_5	-0.010	0.330	0.045	0.040	0.048	-0.009	0.018	-0.006
RbV_3Sb_5	0.020	0.340	0.036	0.050	0.048	-0.007	0.022	-0.004
CsV_3Sb_5	0.080	0.365	0.010	0.060	0.048	-0.006	0.030	-0.004
CsV_3Sb_5 (SD+ISD)	0.100	0.380	0.025	0.060	0.048	-0.006	0.030	-0.004

VHSs near the Fermi level is known to contribute to various phenomena, such as superconductivity [71, 72, 73], magnetism [74, 75], and nematicity [76]. Nevertheless, the origin of such intricate CDW order in AV_3Sb_5 remains a topic of ongoing research.

In this paper, we use first-principles density functional theory (DFT) and a tight-binding (TB) model to investigate the influence of interlayer interactions on the electronic structure of AV_3Sb_5 ($A = K, Rb, Cs$) kagomé systems, with a particular emphasis on changes in the VHS near the Fermi level depending on various 3D CDW stacking configurations. We develop a minimal 3D TB model that effectively captures interlayer interactions. This model faithfully reproduces the DFT bands and density of states for all three AV_3Sb_5 compounds. Our investigation reveals the critical role of interlayer interactions among vanadium layers in describing the diverging electronic density of states near the Fermi level, which influences the ground state 3D CDW order. Based on our comprehensive calculations, we demonstrate that in 3D CDW structures without a π -phase shift, the VHS is close to the Fermi level. However, in the ISD structure with lateral π -phase shift stacking, the VHS moves sufficiently below the Fermi level, stabilizing this configuration as the ground state 3D CDW order. Our findings contribute to the understanding of the origin of 3D CDW orders observed in kagomé metals.

2. Methods

2.1. DFT methods

To investigate the electronic structures of AV_3Sb_5 ($A = K, Rb, Cs$), we performed first-principles calculations based on density functional theory (DFT) as implemented in the Vienna *ab initio* simulation package (VASP) [77, 78, 79, 80]. We used Perdew-Burke-Ernzerhof (PBE) [81] within the generalized gradient approximation (GGA) to describe the exchange and correlation functionals. We used projector augmented wave (PAW) pseudopotentials [82] and plane basis set with an energy cutoff of 300 eV. We applied the zero-damping DFT-D3 [83] van der Waals correction throughout our calculations. Brillouin zone integration was performed using the Γ -centered sampling with $11 \times 11 \times 13$ k -mesh for the $2 \times 2 \times 1$ unit cell and $11 \times 11 \times 7$ k -mesh for the $2 \times 2 \times 2$ unit cell. The geometry of the structures was optimised until all forces are below 0.01 eV/Å. We used the Wannier90 package [84]

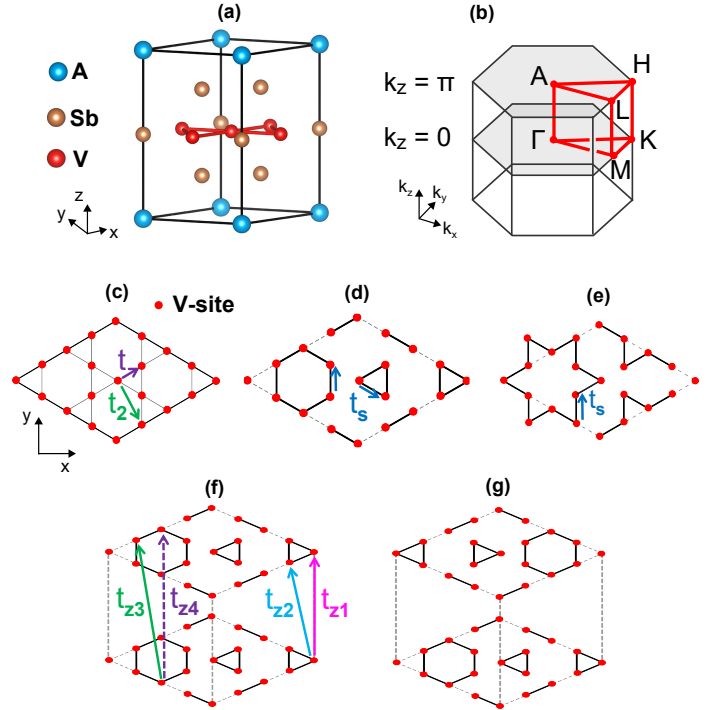


Figure 1: (a) Primitive $1 \times 1 \times 1$ unit cell of AV_3Sb_5 ($A = K, Rb, Cs$). (b) Hexagonal Brillouin zone. The $k_z = 0$ and $k_z = \pi$ planes are indicated by grey planes. High-symmetry lines and points are colored red. (c) Top view of the vanadium kagomé layer in the $2 \times 2 \times 1$ cell. Red circles represent the vanadium sites. (d) Inverse star of David and (e) Star of David CDW structures in the in-plane kagomé layer. The connected solid lines represent the shortened bonding lengths compared to the pristine structure. (f, g) $2 \times 2 \times 2$ supercell (f) without π phase shift and (g) with π phase shift stackings of ISD layers along the out-of-plane direction. Arrows schematically delineate the hopping of electrons via the corresponding hopping parameters t , t_2 , t_s , t_{z1} , t_{z2} , t_{z3} , and t_{z4} , respectively.

to generate maximally localized Wannier functions (MLWFs) [85, 86, 87], enabling us to obtain the Fermi surface (FS). Subsequently, we extracted constant energy contours from the FS using the FermiSurfer tool [88].

2.2. Tight-binding model

We construct a 24-band tight-binding model that describes the d_{xy} orbitals (in local coordinates) of the vanadium kagomé layers within a $2 \times 2 \times 2$ supercell. The d_{xy} -orbital tight-binding model gives rise to the A_g irreducible representation for the VHS state at the M point

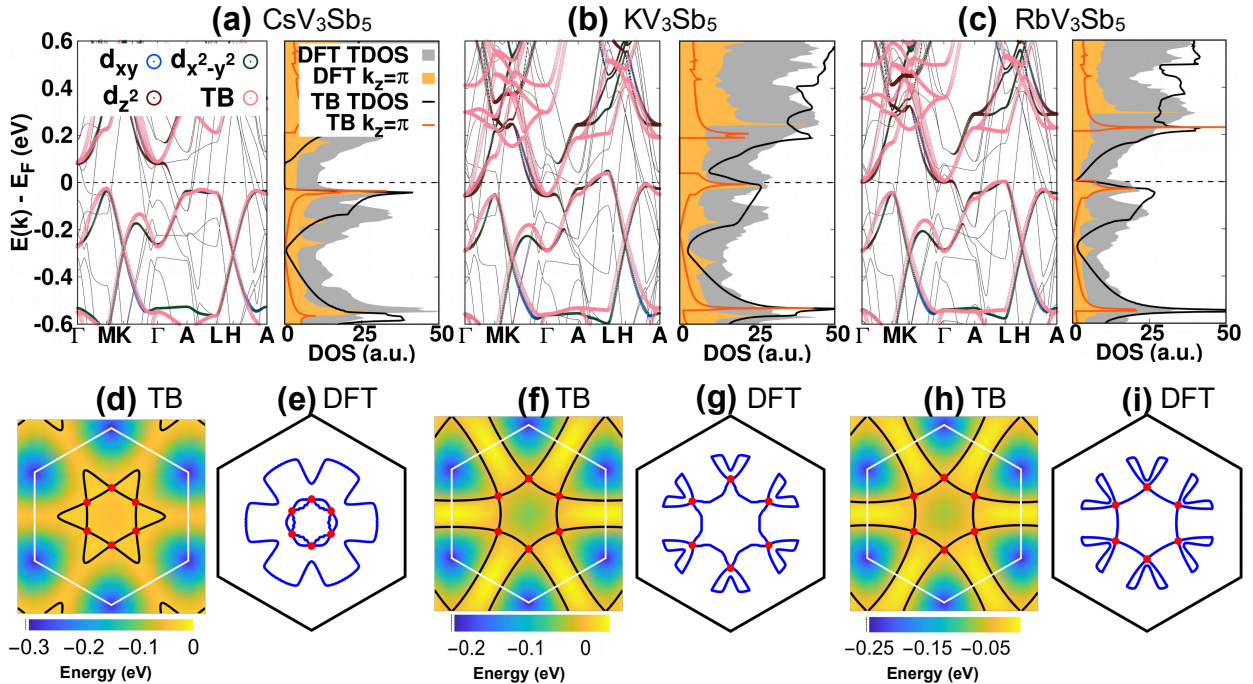


Figure 2: (a-c) DFT and TB electronic band structures and density of states (DOS) of the $2 \times 2 \times 1$ ISD structures for (a) CsV₃Sb₅, (b) KV₃Sb₅, and (c) RbV₃Sb₅. In these plots, the DFT band structure is projected onto the d_{xy} , $d_{x^2-y^2}$, and d_{z^2} orbitals (in global coordinates) of vanadium atoms, with the magnitude of open circles proportional to the projected weight. For the DOS, we display both the total DOS (TDOS) and the DOS resolved for the $k_z = \pi$ plane. (d,e) Constant energy contours in the $k_z = \pi$ plane for CsV₃Sb₅ obtained from (d) the TB and (e) the DFT calculations. (f,g) and (h,i) show the same as (d,e) but for KV₃Sb₅ and RbV₃Sb₅, respectively. Energy contours using TB (DFT) are taken at -0.0346 (-0.0364) eV, -0.0070 (0.0097) eV, and -0.0287 (-0.0336) eV for CsV₃Sb₅, KV₃Sb₅, and RbV₃Sb₅, respectively. Red colored dots designate the VHS points in the energy contours.

near the Fermi level in the $1 \times 1 \times 1$ pristine structure (see also Ref. [31]). The amplitude of the hopping parameters was determined so that the DFT bands were reproduced. We introduce a twelve-component spinor in the $2 \times 2 \times 1$ unit cell of the vanadium kagomé layer and write the tight-binding Hamiltonian as

$$H = \sum_{\mathbf{k}} \Psi_{\mathbf{k}}^\dagger \mathcal{H}(\mathbf{k}) \Psi_{\mathbf{k}}.$$

The spinor $\Psi_{\mathbf{k}}$ is composed of three different sublattices $A_{\mathbf{k}}$, $B_{\mathbf{k}}$, and $C_{\mathbf{k}}$, where

$$\alpha_{\mathbf{k}} = (\alpha_{1\mathbf{k}}, \alpha_{2\mathbf{k}}, \alpha_{3\mathbf{k}}, \alpha_{4\mathbf{k}})^T$$

for $\alpha = A, B, C$. The α_i refers to the α sublattice in the i -th site within the $2 \times 2 \times 1$ supercell, as shown in Fig. 1 (see also Fig. S1 in the Supplemental Information). Our minimal TB Hamiltonian can be grouped into

$$\begin{aligned} \mathcal{H}(\mathbf{k}) &= \mathcal{H}_{\text{NN}}(\mathbf{k}) + \mathcal{H}_{\text{NNN}}(\mathbf{k}) \\ &+ \mathcal{H}_{\text{SD}}(\mathbf{k}) + \mathcal{H}_{\text{ISD}}(\mathbf{k}) + \mathcal{H}^{\text{out}}(\mathbf{k}) \end{aligned} \quad (1)$$

Here, $\mathcal{H}_{\text{NN}}(\mathbf{k})$ and $\mathcal{H}_{\text{NNN}}(\mathbf{k})$ are the nearest-neighbor (NN) and next-nearest-neighbor (NNN) hopping matrices within the 2D kagomé layer. $\mathcal{H}_{\text{SD}}(\mathbf{k})$ and $\mathcal{H}_{\text{ISD}}(\mathbf{k})$ are the NN hopping matrices that describe the SD and ISD type distortions [Figs. 1(d) and 1(e)], respectively. $\mathcal{H}^{\text{out}}(\mathbf{k})$ accounts

for the interlayer hoppings between out-of-plane vanadium sites [Fig. 1(f)], specified by the level of nearest neighbors as

$$\begin{aligned} \mathcal{H}^{\text{out}}(\mathbf{k}) &= \mathcal{H}_{\text{NN}}^{3\text{D}}(\mathbf{k}) + \mathcal{H}_{\text{NNN}}^{3\text{D}}(\mathbf{k}) \\ &+ \mathcal{H}_{\text{NNNN}}^{3\text{D}}(\mathbf{k}) + \mathcal{H}_{\text{NNNNN}}^{3\text{D}}(\mathbf{k}) \end{aligned} \quad (2)$$

The detailed forms of these matrices are given in the Supplemental Information². Previous tight-binding models have been developed to accurately describe multiple VHSs near the Fermi energy [89, 90] and band topology [91], including the Sb p orbital. Our model differs from these models in that it excludes the Sb p orbital and focuses on generically describing a single VHS near the Fermi level originating from the $k_z = \pi$ plane that is sensitive to the 3D CDW formation. This approach focuses on the instability in the $2 \times 2 \times 1$ supercell structure to explore the instability in the 3D stacking configurations of the CDW phases.

3. Results and Discussion

Let us first briefly introduce the atomic structure of AV₃Sb₅ in the pristine and CDW phases. The pristine

²See the detailed forms of matrices of the tight-binding Hamiltonian

phase of AV_3Sb_5 has a layered hexagonal structure (space group $P6/mmm$, No. 191). This structure features specific atomic positions and stacking configurations, shown in Fig. 1(a). The corresponding hexagonal Brillouin zone is depicted in Fig. 1(b). In the pristine structure, the alkali atoms A occupy the Wyckoff position $1a(0, 0, 0)$. The kagomé layers consist of vanadium atoms located at the Wyckoff position $3g(\frac{1}{2}, \frac{1}{2}, \frac{1}{2})$, interleaved with a hexagonal lattice of Sb atoms situated at the Wyckoff position $1b(0, 0, \frac{1}{2})$. Another layer of Sb atoms with a honeycomb structure resides at Wyckoff position $4h(\frac{2}{3}, \frac{1}{3}, z_{Sb})$. The atomic parameters slightly vary depending on the A atom. The optimized structural parameters, in good agreement with the experimental parameters, are listed in Table 2.

For the CDW structures, we consider both ISD and SD type distortions observed in the experiment [67]. Figures 1(c-e) show top views of the vanadium kagomé layer for the pristine, the ISD, and SD structures, respectively. Compared to the 1×1 pristine structure, the ISD and SD distortions expand to a 2×2 in-plane periodicity. The stacking configurations of non- π -phase shifted and π -phase shifted ISD+ISD type kagomé layers along the out-of-plane c -direction are illustrated in Figs. 1(f) and 1(g). The non- π -shifted stacking configuration has a lattice periodicity of $2 \times 2 \times 1$ with a uniform atomic arrangement without any in-plane translation between the adjacent kagomé layers. Conversely, the π -shifted configuration involves a half translation of the in-plane unit vectors between adjacent kagomé layers, leading to a $2 \times 2 \times 2$ periodicity. In line with the previous calculations [60, 92], our DFT total energy calculations show that the π -shifted $2 \times 2 \times 2$ ISD+ISD phase is energetically more favorable than the non- π -shifted phase for all three alkali atoms ($A = K, Rb, Cs$). The energy decreases by 16.8, 16.6, and 10.6 meV per $2 \times 2 \times 1$ unit cell for the π -shifted phase compared to the non- π -shifted phase in KV_3Sb_5 , RbV_3Sb_5 , and CsV_3Sb_5 , respectively.

Our TB model can generically reproduce the DFT bands for various CDW stacking configurations. A specific set of TB parameters accurately replicates the DFT bands for the d_{xy} , $d_{3z^2-r^2}$, and $d_{x^2-y^2}$ orbitals (in global coordinates) near the Fermi level for both the π -shifted and non- π -shifted stacking configurations of ISD or SD structures. Figures 2(a-c) depict the electronic band structures and the density of states obtained using both DFT and TB for the $2 \times 2 \times 1$ non- π -shifted ISD structure for all three

Table 2: Structural parameters for pristine AV_3Sb_5 ($A = Cs, K, Rb$) obtained from DFT. The lattice parameters (a, c) are given in the Angstrom unit, while z_{Sb} is provided in the fractional unit of c . Experimental values from Ref. [16] are given in parenthesis for comparison.

A	a [Å]	c [Å]	z_{Sb} [c]
Cs	5.439 (5.495)	9.326 (9.309)	0.742 (0.742)
K	5.411 (5.482)	8.893 (8.948)	0.756 (0.754)
Rb	5.425 (5.472)	9.114 (9.073)	0.749 (0.750)

Table 3: Relative total energy (in meV per $2 \times 2 \times 1$ unit cell) for various CDW stacking configurations. The total energy of the non- π -shifted ISD stacking is set to zero.

	non- π -shift ISD+ISD	non- π -shift SD+ISD	π -shift ISD+ISD
CsV_3Sb_5	0.0	15.4	-10.6

alkali metals. Our TB bands (colored pink) closely match the DFT bands of vanadium d_{xy} , $d_{3z^2-r^2}$, and $d_{x^2-y^2}$ orbitals (colored blue, brown, and green, respectively) for all three alkali metals. The employed sets of TB parameters for AV_3Sb_5 ($A = K, Rb, Cs$) are presented in Table 1. The out-of-plane hopping parameters in our minimal vanadium TB models show substantial magnitudes, which effectively capture the three-dimensional nature of these systems. Notably, the nearest-neighbor (NN) hopping parameter along the out-of-plane direction, t_{z1} , is larger than the in-plane next-nearest-neighbor (NNN) hopping parameter, t_2 , for all three systems. Additionally, the NNNN out-of-plane hopping parameter t_{z3} is larger than the NNN out-of-plane hopping parameter t_{z2} , which we attribute to the weak overlap between the NNN sites.

Our comprehensive DFT and TB calculations reveal a sharp peak in the DOS just below the Fermi level for the $2 \times 2 \times 1$ non- π -shifted ISD structure in all three compounds, mainly attributed to the VHS at $k_z = \pi$. The constant energy contours in the $k_z = \pi$ plane, obtained by both DFT [Figs. 2(e,g,i)] and TB [Figs. 2(d,f,h)] calculations, show six symmetry-related van Hove saddle points, with one located along the $A - H$ direction and the other five along other symmetry-related high symmetry lines. The VHSs are identified by the crossing points (colored red) in the constant energy contour, which satisfy two conditions: (i) zero gradient of energy dispersion $\nabla_{\mathbf{k}} E_{\mathbf{k}} = 0$ and (ii) a negative value of the Hessian determinant $\frac{\partial^2 E_{\mathbf{k}}}{\partial k_x^2} \frac{\partial^2 E_{\mathbf{k}}}{\partial k_y^2} - \frac{\partial^2 E_{\mathbf{k}}}{\partial k_x \partial k_y} \frac{\partial^2 E_{\mathbf{k}}}{\partial k_y \partial k_x} < 0$. These VHSs at the $k_z = \pi$ plane primarily contribute to the large DOS below the Fermi level, as consistently confirmed by both DFT and TB calculations [Figs. 2(a-c)], indicating that the d_{xy} , $d_{3z^2-r^2}$, and $d_{x^2-y^2}$ orbitals of vanadium atoms (in global coordinates) are responsible for electronic instabilities near the Fermi level in the non- π -shifted CDW order.

We conduct further analysis on the VHSs in the $2 \times 2 \times 1$ non- π -shifted ISD structure. The VHSs are classified as type-II, as they reside off time-reversal invariant momenta [31, 93, 94]. The explicitly calculated Hessian determinant values using TB models for these type-II VHSs are $-0.327 \text{ eV}\text{\AA}^2$, $-1.716 \text{ eV}\text{\AA}^2$, and $-1.408 \text{ eV}\text{\AA}^2$ for CsV_3Sb_5 , KV_3Sb_5 , and RbV_3Sb_5 , respectively. The value is quite close to zero in the case of Cs, in line with the flat-like dispersion along the $A - L$ direction [Fig. 2(a)] and quasi-flat energy band landscape across broader regions near the A point [Fig. 2(d)], a distinct feature from the other two systems. Consequently, the VHSs in the $2 \times 2 \times 1$ ISD CDW phase in the CsV_3Sb_5 system are

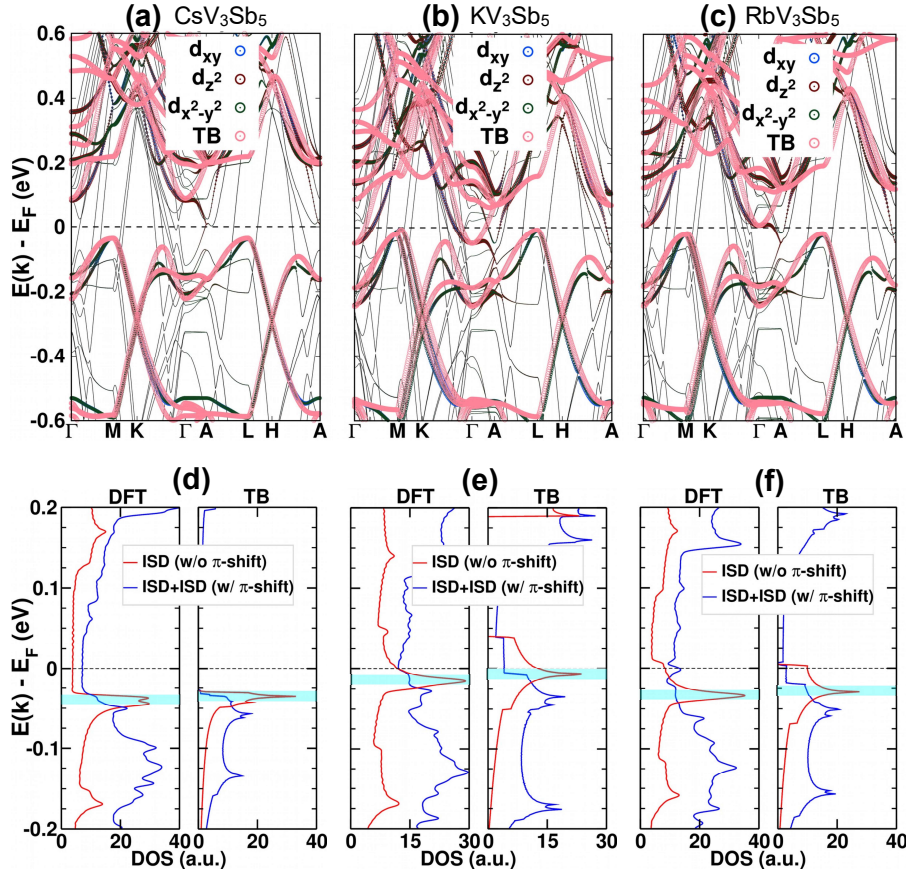


Figure 3: (a-c) DFT and TB electronic band structures and DOS of the $2 \times 2 \times 2$ π -phase shift ISD+ISD structures for (a) CsV₃Sb₅, (b) KV₃Sb₅, and (c) RbV₃Sb₅. The orbital-projected DFT band structures, with the radius of open circles proportional to the projected weight, are overlaid with the TB band structures. (d-f) The $k_z = 0$ (and the $k_z = \pi$) plane-resolved DOS of the $2 \times 2 \times 2$ π -shifted ISD+ISD (and the $2 \times 2 \times 1$ non- π -shifted ISD) structures obtained using DFT and TB for (d) CsV₃Sb₅, (e) KV₃Sb₅, and (f) RbV₃Sb₅. The DFT DOSs are normalized per unit cell. We note that ISD+ISD has double the number of atoms compared to the ISD.

further characterized as higher-order-like VHSs, where a higher-order VHS is defined by a zero value of the Hessian determinant [94], serving as sources of diverse intriguing many-body phenomena [94, 95]. We note that both the type-II and higher-order like VHSs found in our study are different from those studied in the pristine phase at the $k_z = 0$ plane in the monolayer limit [31] and in the bulk CsV₃Sb₅ system [29], respectively. This suggests that the VHSs still play an important role in stacking-dependent 3D CDW phases.

We examine the π -phase shift stacking effect on the electronic structures of AV₃Sb₅. We consider the $2 \times 2 \times 2$ π -shifted ISD+ISD structure where alternating ISD layers along the c -direction are relatively shifted by a π -phase from each other [Fig. 1(g)]. The band dispersion and DOS for the $2 \times 2 \times 2$ π -shifted ISD+ISD structure for all three alkali metals are shown in Fig. 3. The same TB parameters used for the $2 \times 2 \times 1$ non- π -shifted ISD structure yield TB bands in good agreement with the DFT bands of vanadium d_{xy} , $d_{3z^2-r^2}$, and $d_{x^2-y^2}$ orbitals [Figs. 3(a-c)]. To track the changes in energy bands under the π -phase shift, we compare the energy bands at $k_z = 0$ for the $2 \times 2 \times 2$

structure with those at both the $k_z = 0$ and $k_z = \pi$ planes for the $2 \times 2 \times 1$ structure. This comparison is necessary because, when a π -phase shift occurs, the energy bands at the $k_z = \pi$ plane in the $2 \times 2 \times 1$ CDW fold into the $k_z = 0$ plane in the $2 \times 2 \times 2$ CDW, resulting in a doubling of the number of energy bands. The overall band dispersions at the $k_z = 0$ plane of the $2 \times 2 \times 2$ ISD+ISD structure [Fig. 3(a-c)] are similar to those of the $2 \times 2 \times 1$ ISD structure at both the $k_z = 0$ and $k_z = \pi$ planes [Figs. 2(a-c)]. However, a significant difference occurs in the flat-like dispersions along the $A - L$ line in the $2 \times 2 \times 1$ structure. In the $2 \times 2 \times 2$ structure, these flat-like dispersions become more dispersive under the π -phase shift, as seen along the $\Gamma - M$ line. Consequently, the DOS in the π -shifted ISD+ISD structure exhibits a depletion near the Fermi level compared to the non- π -shifted ISD structure, indicating the lifting of the VHSs due to the π -phase shift [Figs. 3(d-f)]. This leads to electrons occupying lower energy levels, thereby stabilizing the π -shifted structure. The in-plane d_{xy} , $d_{3z^2-r^2}$, and $d_{x^2-y^2}$ orbitals capture essential changes in the DOS under the out-of-plane π -phase shift, highlighting their crucial roles in stabilizing the ground

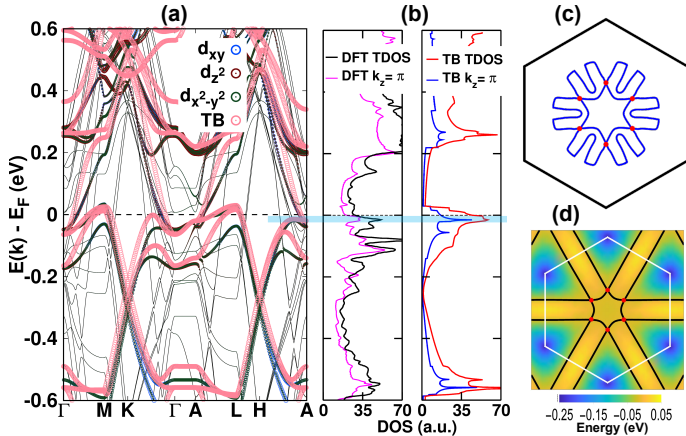


Figure 4: Electronic structure of the $2 \times 2 \times 2$ SD+ISD structure without a π -phase shift for CsV_3Sb_5 . (a) The orbital-projected DFT band structure, overlaid with the TB band structure. (b) Total density of states (TDOS) and $k_z = \pi$ plane-resolved DOS from DFT and TB. (c,d) Constant energy contours in the $k_z = \pi$ plane obtained using (c) DFT and (d) TB, respectively. Energy contours are displayed at energy values of -0.009 eV for TB and -0.012 eV for DFT calculations. Red colored dots designate the VHS points in the energy contours.

state 3D CDW order.

We finalize our discussion by speculating on the significance of our findings in alternating SD and ISD distorted layers, which are observed as part of the $2 \times 2 \times 4$ CDW structure in CsV_3Sb_5 [52, 67, 96]. The existence of the $2 \times 2 \times 4$ CDW structure in CsV_3Sb_5 was controversial, and was later found to be sensitive to growth conditions such as chemical disorder and thermal annealing [68, 69, 70]. For the structural model, initial experiment suggested alternating ISD layers followed by three SD distorted layers along the c -direction without any π -phase shift between adjacent kagomé layers [67]. However, subsequent studies [69, 70, 96] propose various stacking configurations, including complex stacking arrangements of ISD layers without alternating SD layers in the $2 \times 2 \times 4$ CDW structure. Our total energy calculations show that the π -shift stacking remains favorable over the SD+ISD stacking (Table 3), consistent with previous DFT calculations [60, 69]. Our calculations of the band structure, DOS, and constant energy contour for CsV_3Sb_5 with alternating SD and ISD layers (Fig. 4), reveal a sharp DOS peak just below the Fermi level originating from the $k_z = \pi$ plane, attributed to the VHSs. This observation potentially supports the $2 \times 2 \times 4$ structural model with an ISD+ISD π -shift structure, as the electronic instability is indicated in the alternating SD+ISD structure and the additional periodicity doubling along the c -axis may relieve this diverging DOS at the Fermi level as in the case of the $2 \times 2 \times 1$ to $2 \times 2 \times 2$ transition.

4. Conclusion

Our comprehensive investigation, employing DFT and tight-binding calculations, delves into the stacking-dependent electronic structures of 3D CDW structures in AV_3Sb_5 . Our findings unveil the electronic origin of out-of-plane CDW ordering, highlighting the critical role of interlayer coupling in electronic instabilities near the Fermi level. A crucial aspect of our findings centers around the instability inherent in the $2 \times 2 \times 1$ ISD structure, attributed to the intense density of states originating from the $k_z = \pi$ plane at or near the Fermi level. This enhanced density of states is associated with the presence of type-II van Hove singularities. However, upon the 3D stacking of ISD layers along the c -direction with a π -phase shift, we observe a substantial renormalization of the density of states at the Fermi level, leading to the disappearance of the van Hove singularities and thus stabilizing the 3D π -shifted ISD+ISD CDW ground state. Furthermore, our analysis highlights that the alternative stacking of ISD+SD layers in CsV_3Sb_5 also presents electronic instabilities near the Fermi level, making it energetically less favorable than the ISD+ISD π -shifted configuration.

Additionally, we have formulated an effective 3D tight-binding model that captures the essential physics of AV_3Sb_5 kagomé systems. This model serves as a valuable platform for further investigation of 3D interlayer coupling effects on novel phenomena observed in AV_3Sb_5 kagomé metals. We anticipate that this approach will uncover new exotic physics beyond the current studies limited to 2D kagomé models, such as three-dimensional chiral flux order and three-dimensional electronic nematicity.

We conclude by comparing our study to a previous one [89, 97] that introduces a comprehensive tight-binding model for the four d orbitals of V and the p_z orbital of Sb, which is essential for describing the energies of four VHSs near the Fermi level in the $k_z = 0$ plane under various strains and might be useful for describing all VHSs throughout the BZ. While this model is comprehensive, our simple model focuses on the d_{xy} orbitals and effectively describes the VHS that governs the low-energy electronic structure in the $k_z = \pi$ plane without 3D CDW. We believe our simplified TB theory offers a practical approach for future research on interacting Hamiltonians and complex systems, such as twisted bilayer AV_3Sb_5 systems.

Data availability statement

All data are included within the article and its supplementary materials.

Declaration of competing interest

The authors declare that there are no competing financial interests or personal relationships that could have influenced the work reported in this paper.

Acknowledgments

Y.K. acknowledges the support from the National Research Foundation (NRF) of Korea under grant number NRF-2021R1A2C1013871. The Korea Institute of Science and Technology Information (KISTI) (KSC-2021-CRE-0116) provided the computational resource.

Appendix A. Supplementary data

Supplementary data to this article can be found online at

References

- [1] J.-W. Rhim, K. Kim, B.-J. Yang, Quantum distance and anomalous Landau levels of flat bands, *Nature* 584 (7819) (2020) 59–63.
<http://dx.doi.org/10.1038/s41586-020-2540-1>
- [2] M. Li, D. Zhirihin, M. Gorchach, X. Ni, D. Filonov, A. Slobozhanyuk, A. Alù, A. B. Khanikaev, Higher-order topological states in photonic kagome crystals with long-range interactions, *Nat. Photonics* 14 (2) (2020) 89–94.
<http://dx.doi.org/10.1038/s41566-019-0561-9>
- [3] M. Kang, S. Fang, L. Ye, H. C. Po, J. Denlinger, C. Jozwiak, A. Bostwick, E. Rotenberg, E. Kaxiras, J. G. Checkelsky, R. Comin, Topological flat bands in frustrated kagome lattice CoSn , *Nat. Commun.* 11 (1) (2020) 4004.
<http://dx.doi.org/10.1038/s41467-020-17465-1>
- [4] W.-H. Ko, P. A. Lee, X.-G. Wen, Doped kagome system as exotic superconductor, *Phys. Rev. B* 79 (2009) 214502.
<https://link.aps.org/doi/10.1103/PhysRevB.79.214502>
- [5] S.-L. Yu, J.-X. Li, Chiral superconducting phase and chiral spin-density-wave phase in a Hubbard model on the kagome lattice, *Phys. Rev. B* 85 (2012) 144402.
<https://link.aps.org/doi/10.1103/PhysRevB.85.144402>
- [6] M. L. Kiesel, C. Platt, R. Thomale, Unconventional Fermi surface instabilities in the kagome Hubbard model, *Phys. Rev. Lett.* 110 (2013) 126405.
<https://link.aps.org/doi/10.1103/PhysRevLett.110.126405>
- [7] W.-S. Wang, Z.-Z. Li, Y.-Y. Xiang, Q.-H. Wang, Competing electronic orders on kagome lattices at van Hove filling, *Phys. Rev. B* 87 (2013) 115135.
<https://link.aps.org/doi/10.1103/PhysRevB.87.115135>
- [8] S. Yan, D. A. Huse, S. R. White, Spin-liquid ground state of the $s = 1/2$ kagome Heisenberg antiferromagnet, *Science* 332 (6034) (2011) 1173–1176.
<http://dx.doi.org/10.1126/science.1201080>
- [9] T.-H. Han, J. S. Helton, S. Chu, D. G. Nocera, J. A. Rodriguez-Rivera, C. Broholm, Y. S. Lee, Fractionalized excitations in the spin-liquid state of a kagome-lattice antiferromagnet, *Nature* 492 (7429) (2012) 406–410.
<http://dx.doi.org/10.1038/nature11659>
- [10] J.-X. Yin, B. Lian, M. Z. Hasan, Topological kagome magnets and superconductors, *Nature* 612 (7941) (2022) 647–657.
<https://doi.org/10.1038/s41586-022-05516-0>
- [11] M. Fu, T. Imai, T.-H. Han, Y. S. Lee, Evidence for a gapped spin-liquid ground state in a kagome Heisenberg antiferromagnet, *Science* 350 (6261) (2015) 655–658.
<https://www.science.org/doi/abs/10.1126/science.aab2120>
- [12] Y. Zhou, K. Kanoda, T.-K. Ng, Quantum spin liquid states, *Rev. Mod. Phys.* 89 (2) (2017) 025003.
<https://link.aps.org/doi/10.1103/RevModPhys.89.025003>
- [13] M. Kang, L. Ye, S. Fang, J.-S. You, A. Levitan, M. Han, J. I. Facio, C. Jozwiak, A. Bostwick, E. Rotenberg, et al., Dirac fermions and flat bands in the ideal kagome metal FeSn , *Nat. Mater.* 19 (2) (2020) 163–169.
<https://doi.org/10.1038/s41563-019-0531-0>
- [14] Z. Lin, J.-H. Choi, Q. Zhang, W. Qin, S. Yi, P. Wang, L. Li, Y. Wang, H. Zhang, Z. Sun, et al., Flatbands and emergent ferromagnetic ordering in Fe_3Sn_2 kagome lattices, *Phys. Rev. Lett.* 121 (9) (2018) 096401.
<https://link.aps.org/doi/10.1103/PhysRevLett.121.096401>
- [15] H. Huang, L. Zheng, Z. Lin, X. Guo, S. Wang, S. Zhang, C. Zhang, Z. Sun, Z. Wang, H. Weng, et al., Flat-band-induced anomalous anisotropic charge transport and orbital magnetism in kagome metal CoSn , *Phys. Rev. Lett.* 128 (9) (2022) 096601.
<https://link.aps.org/doi/10.1103/PhysRevLett.128.096601>
- [16] B. R. Ortiz, L. C. Gomes, J. R. Morey, M. Winiarski, M. Bordelon, J. S. Mangum, I. W. H. Oswald, J. A. Rodriguez-Rivera, J. R. Neilson, S. D. Wilson, E. Ertekin, T. M. McQueen, E. S. Toberer, New kagome prototype materials: discovery of KV_3Sb_5 , RbV_3Sb_5 , and CsV_3Sb_5 , *Phys. Rev. Mater.* 3 (2019) 094407.
<https://link.aps.org/doi/10.1103/PhysRevMaterials.3.094407>
- [17] B. R. Ortiz, S. M. L. Teicher, Y. Hu, J. L. Zuo, P. M. Sarte, E. C. Schueller, A. M. M. Abeykoon, M. J. Krogstad, S. Rosenkranz, R. Osborn, R. Seshadri, L. Balents, J. He, S. D. Wilson, CsV_3Sb_5 : A \mathbb{Z}_2 topological kagome metal with a superconducting ground state, *Phys. Rev. Lett.* 125 (2020) 247002.
<https://link.aps.org/doi/10.1103/PhysRevLett.125.247002>
- [18] S. D. Wilson, B. R. Ortiz, AV_3Sb_5 kagome superconductors, *Nat. Rev. Mater.* (2024).
<https://doi.org/10.1038/s41578-024-00677-y>
- [19] H. Yang, Z. Zhao, X.-W. Yi, J. Liu, J.-Y. You, Y. Zhang, H. Guo, X. Lin, C. Shen, H. Chen, et al., Titanium-based kagome superconductor CsTi_3Bi_5 and topological states, arXiv preprint arXiv:2209.03840 (2022).
<https://arxiv.org/abs/2209.03840>
- [20] D. Werhahn, B. R. Ortiz, A. K. Hay, S. D. Wilson, R. Seshadri, D. Johrendt, The kagomé metals RbTi_3Bi_5 and CsTi_3Bi_5 , *Z. Naturforsch. B* 77 (11-12) (2022) 757–764.
<https://doi.org/10.1515/znb-2022-0125>
- [21] B. Liu, M.-Q. Kuang, Y. Luo, Y. Li, C. Hu, J. Liu, Q. Xiao, X. Zheng, L. Huai, S. Peng, et al., Tunable van Hove singularity without structural instability in kagome metal CsTi_3Bi_5 , *Phys. Rev. Lett.* 131 (2) (2023) 026701.
<https://link.aps.org/doi/10.1103/PhysRevLett.131.026701>
- [22] G. Pokharel, S. M. L. Teicher, B. R. Ortiz, P. M. Sarte, G. Wu, S. Peng, J. He, R. Seshadri, S. D. Wilson, Electronic properties of the topological kagome metals YV_6Sn_6 and GdV_6Sn_6 , *Phys. Rev. B* 104 (2021) 235139.
<https://link.aps.org/doi/10.1103/PhysRevB.104.235139>
- [23] H. W. S. Arachchige, W. R. Meier, M. Marshall, T. Matsuoka, R. Xue, M. A. McGuire, R. P. Hermann, H. Cao, D. Mandrus, Charge density wave in kagome lattice intermetallic ScV_6Sn_6 , *Phys. Rev. Lett.* 129 (2022) 216402.
<https://link.aps.org/doi/10.1103/PhysRevLett.129.216402>
- [24] K. Wang, S. Chen, S.-W. Kim, B. Monserrat, Origin of competing charge density waves in kagome metal ScV_6Sn_6 , arXiv preprint arXiv:2403.17058 (2024).
<https://arxiv.org/abs/2403.17058>
- [25] X. Teng, L. Chen, F. Ye, E. Rosenberg, Z. Liu, J.-X. Yin, Y.-X. Jiang, J. S. Oh, M. Z. Hasan, K. J. Neubauer, B. Gao, Y. Xie, M. Hashimoto, D. Lu, C. Jozwiak, A. Bostwick, E. Rotenberg, R. J. Birgeneau, J.-H. Chu, M. Yi, P. Dai, Discovery of charge density wave in a kagome lattice antiferromagnet, *Nature* 609 (7927) (2022) 490–495.
<https://doi.org/10.1038/s41586-022-05034-z>
- [26] X. Teng, J. S. Oh, H. Tan, L. Chen, J. Huang, B. Gao, J.-X. Yin, J.-H. Chu, M. Hashimoto, D. Lu, C. Jozwiak, A. Bostwick, E. Rotenberg, G. E. Granroth, B. Yan, R. J. Birgeneau, P. Dai, M. Yi, Magnetism and charge density wave order in kagome fege, *Nature Physics* 19 (6) (2023) 814–822.
<https://doi.org/10.1038/s41567-023-01985-w>

- [27] J.-X. Yin, Y.-X. Jiang, X. Teng, M. S. Hossain, S. Mardanya, T.-R. Chang, Z. Ye, G. Xu, M. M. Denner, T. Neupert, B. Lienhard, H.-B. Deng, C. Setty, Q. Si, G. Chang, Z. Guguchia, B. Gao, N. Shumiya, Q. Zhang, T. A. Cochran, D. Multer, M. Yi, P. Dai, M. Z. Hasan, Discovery of charge order and corresponding edge state in kagome magnet FeGe, *Phys. Rev. Lett.* 129 (2022) 166401.
<https://link.aps.org/doi/10.1103/PhysRevLett.129.166401>
- [28] X. Wu, T. Schwemmer, T. Müller, A. Consiglio, G. Sangiovanni, D. Di Sante, Y. Iqbal, W. Hanke, A. P. Schnyder, M. M. Denner, M. H. Fischer, T. Neupert, R. Thomale, Nature of unconventional pairing in the kagome superconductors AV_3Sb_5 ($A = K, Rb, Cs$), *Phys. Rev. Lett.* 127 (2021) 177001.
<https://link.aps.org/doi/10.1103/PhysRevLett.127.177001>
- [29] M. Kang, S. Fang, J.-K. Kim, B. R. Ortiz, S. H. Ryu, J. Kim, J. Yoo, G. Sangiovanni, D. Di Sante, B.-G. Park, et al., Twofold van hove singularity and origin of charge order in topological kagome superconductor CsV_3Sb_5 , *Nat. Phys.* 18 (3) (2022) 301–308.
<https://doi.org/10.1038/s41567-021-01451-5>
- [30] Y. Hu, X. Wu, B. R. Ortiz, S. Ju, X. Han, J. Ma, N. C. Plumb, M. Radovic, R. Thomale, S. D. Wilson, A. P. Schnyder, M. Shi, Rich nature of van hove singularities in kagome superconductor CsV_3Sb_5 , *Nat. Commun.* 13 (1) (2022) 2220.
<https://doi.org/10.1038/s41467-022-29828-x>
- [31] S.-W. Kim, H. Oh, E.-G. Moon, Y. Kim, Monolayer kagome metals AV_3Sb_5 , *Nat. Commun.* 14 (1) (2023) 591.
<https://doi.org/10.1038/s41467-023-36341-2>
- [32] T. Neupert, M. M. Denner, J.-X. Yin, R. Thomale, M. Z. Hasan, Charge order and superconductivity in kagome materials, *Nat. Phys.* 18 (2) (2022) 137–143.
<https://doi.org/10.1038/s41567-021-01404-y>
- [33] K. Jiang, T. Wu, J.-X. Yin, Z. Wang, M. Z. Hasan, S. D. Wilson, X. Chen, J. Hu, Kagome superconductors AV_3Sb_5 ($A = K, Rb, Cs$), *Natl. Sci. Rev.* 10 (2) (2022) nwac199.
<https://doi.org/10.1093/nsr/nwac199>
- [34] S.-Y. Yang, Y. Wang, B. R. Ortiz, D. Liu, J. Gayles, E. Derunova, R. Gonzalez-Hernandez, L. Šmejkal, Y. Chen, S. S. P. Parkin, S. D. Wilson, E. S. Toberer, T. McQueen, M. N. Ali, Giant, unconventional anomalous hall effect in the metallic frustrated magnet candidate, KV_3Sb_5 , *Sci. Adv.* 6 (31) (2020) eabb6003.
<https://www.science.org/doi/abs/10.1126/sciadv.abb6003>
- [35] F. H. Yu, T. Wu, Z. Y. Wang, B. Lei, W. Z. Zhuo, J. J. Ying, X. H. Chen, Concurrence of anomalous hall effect and charge density wave in a superconducting topological kagome metal, *Phys. Rev. B* 104 (2021) L041103.
<https://link.aps.org/doi/10.1103/PhysRevB.104.L041103>
- [36] B. R. Ortiz, P. M. Sarte, E. M. Kenney, M. J. Graf, S. M. L. Teicher, R. Seshadri, S. D. Wilson, Superconductivity in the Z_2 kagome metal KV_3Sb_5 , *Phys. Rev. Mater.* 5 (2021) 034801.
<https://link.aps.org/doi/10.1103/PhysRevMaterials.5.034801>
- [37] Q. Yin, Z. Tu, C. Gong, Y. Fu, S. Yan, H. Lei, Superconductivity and normal-state properties of kagome metal RbV_3Sb_5 single crystals, *Chin. Phys. Lett.* 38 (3) (2021) 037403.
<https://dx.doi.org/10.1088/0256-307X/38/3/037403>
- [38] Y.-X. Jiang, J.-X. Yin, M. M. Denner, N. Shumiya, B. R. Ortiz, G. Xu, Z. Guguchia, J. He, M. S. Hossain, X. Liu, J. Ruff, L. Kautzsch, S. S. Zhang, G. Chang, I. Belopolski, Q. Zhang, T. A. Cochran, D. Multer, M. Litskevich, Z.-J. Cheng, X. P. Yang, Z. Wang, R. Thomale, T. Neupert, S. D. Wilson, M. Z. Hasan, Unconventional chiral charge order in kagome superconductor KV_3Sb_5 , *Nat. Mater.* 20 (10) (2021) 1353–1357.
<https://doi.org/10.1038/s41563-021-01034-y>
- [39] Y.-P. Lin, R. M. Nandkishore, Complex charge density waves at van hove singularity on hexagonal lattices: Haldane-model phase diagram and potential realization in the kagome metals AV_3Sb_5 ($A = K, Rb, Cs$), *Phys. Rev. B* 104 (2021) 045122.
<https://link.aps.org/doi/10.1103/PhysRevB.104.045122>
- [40] T. Park, M. Ye, L. Balents, Electronic instabilities of kagome metals: Saddle points and Landau theory, *Phys. Rev. B* 104 (2021) 035142.
<https://link.aps.org/doi/10.1103/PhysRevB.104.035142>
- [41] X. Feng, K. Jiang, Z. Wang, J. Hu, Chiral flux phase in the kagome superconductor AV_3Sb_5 , *Sci. Bull.* 66 (14) (2021) 1384–1388.
<https://www.sciencedirect.com/science/article/pii/S2095927321003224>
- [42] M. M. Denner, R. Thomale, T. Neupert, Analysis of charge order in the kagome metal AV_3Sb_5 , *Phys. Rev. Lett.* 127 (2021) 217601.
<https://link.aps.org/doi/10.1103/PhysRevLett.127.217601>
- [43] C. Mielke, D. Das, J.-X. Yin, H. Liu, R. Gupta, Y.-X. Jiang, M. Medarde, X. Wu, H. C. Lei, J. Chang, P. Dai, Q. Si, H. Miao, R. Thomale, T. Neupert, Y. Shi, R. Khasanov, M. Z. Hasan, H. Luetkens, Z. Guguchia, Time-reversal symmetry-breaking charge order in a kagome superconductor, *Nature* 602 (7896) (2022) 245–250.
<https://doi.org/10.1038/s41586-021-04327-z>
- [44] C. Guo, C. Putzke, S. Konyzheva, X. Huang, M. Gutierrez-Amigo, I. Errea, D. Chen, M. G. Vergniory, C. Felser, M. H. Fischer, T. Neupert, P. J. W. Moll, Switchable chiral transport in charge-ordered kagome metal CsV_3Sb_5 , *Nature* 611 (7936) (2022) 461–466.
<https://doi.org/10.1038/s41586-022-05127-9>
- [45] Y. Xu, Z. Ni, Y. Liu, B. R. Ortiz, Q. Deng, S. D. Wilson, B. Yan, L. Balents, L. Wu, Three-state nematicity and magneto-optical kerr effect in the charge density waves in kagome superconductors, *Nat. Phys.* 18 (12) (2022) 1470–1475.
<https://doi.org/10.1038/s41567-022-01805-7>
- [46] Y. Xiang, Q. Li, Y. Li, W. Xie, H. Yang, Z. Wang, Y. Yao, H.-H. Wen, Twofold symmetry of c-axis resistivity in topological kagome superconductor CsV_3Sb_5 with in-plane rotating magnetic field, *Nat. Commun.* 12 (1) (2021) 6727.
<https://doi.org/10.1038/s41467-021-27084-z>
- [47] H. Li, H. Zhao, B. R. Ortiz, T. Park, M. Ye, L. Balents, Z. Wang, S. D. Wilson, I. Zeljkovic, Rotation symmetry breaking in the normal state of a kagome superconductor KV_3Sb_5 , *Nat. Phys.* 18 (3) (2022) 265–270.
<https://doi.org/10.1038/s41567-021-01479-7>
- [48] H. Luo, Q. Gao, H. Liu, Y. Gu, D. Wu, C. Yi, J. Jia, S. Wu, X. Luo, Y. Xu, L. Zhao, Q. Wang, H. Mao, G. Liu, Z. Zhu, Y. Shi, K. Jiang, J. Hu, Z. Xu, X. J. Zhou, Electronic nature of charge density wave and electron-phonon coupling in kagome superconductor KV_3Sb_5 , *Nat. Commun.* 13 (1) (2022) 273.
<https://doi.org/10.1038/s41467-021-27946-6>
- [49] H. Li, H. Zhao, B. R. Ortiz, Y. Oey, Z. Wang, S. D. Wilson, I. Zeljkovic, Unidirectional coherent quasiparticles in the high-temperature rotational symmetry broken phase of AV_3Sb_5 kagome superconductors, *Nat. Phys.* 19 (5) (2023) 637–643.
<https://doi.org/10.1038/s41567-022-01932-1>
- [50] S. Wu, B. R. Ortiz, H. Tan, S. D. Wilson, B. Yan, T. Birol, G. Blumberg, Charge density wave order in the kagome metal CsV_3Sb_5 ($A = Cs, Rb, K$), *Phys. Rev. B* 105 (2022) 155106.
<https://link.aps.org/doi/10.1103/PhysRevB.105.155106>
- [51] D. Wulferding, S. Lee, Y. Choi, Q. Yin, Z. Tu, C. Gong, H. Lei, S. Yousuf, J. Song, H. Lee, T. Park, K.-Y. Choi, Emergent nematicity and intrinsic versus extrinsic electronic scattering processes in the kagome metal CsV_3Sb_5 , *Phys. Rev. Res.* 4 (2022) 023215.
<https://link.aps.org/doi/10.1103/PhysRevResearch.4.023215>
- [52] M. Kang, S. Fang, J. Yoo, B. R. Ortiz, Y. M. Oey, J. Choi, S. H. Ryu, J. Kim, C. Jozwiak, A. Bostwick, E. Rotenberg, E. Kaxiras, J. G. Checkelsky, S. D. Wilson, J.-H. Park, R. Comin, Charge order landscape and competition with superconductivity in kagome metals, *Nat. Mater.* 22 (2) (2023) 186–193.
<https://doi.org/10.1038/s41563-022-01375-2>

- [53] Q. Wu, Z. X. Wang, Q. M. Liu, R. S. Li, S. X. Xu, Q. W. Yin, C. S. Gong, Z. J. Tu, H. C. Lei, T. Dong, N. L. Wang, Simultaneous formation of two-fold rotation symmetry with charge order in the kagome superconductor CsV_3Sb_5 by optical polarization rotation measurement, *Phys. Rev. B* 106 (2022) 205109. <https://link.aps.org/doi/10.1103/PhysRevB.106.205109>
- [54] Z. Jiang, H. Ma, W. Xia, Z. Liu, Q. Xiao, Z. Liu, Y. Yang, J. Ding, Z. Huang, J. Liu, Y. Qiao, J. Liu, Y. Peng, S. Cho, Y. Guo, J. Liu, D. Shen, Observation of electronic nematicity driven by the three-dimensional charge density wave in kagome lattice KV_3Sb_5 , *Nano Lett.* 23 (12) (2023) 5625–5633. <https://doi.org/10.1021/acs.nanolett.3c01151>
- [55] L. Nie, K. Sun, W. Ma, D. Song, L. Zheng, Z. Liang, P. Wu, F. Yu, J. Li, M. Shan, D. Zhao, S. Li, B. Kang, Z. Wu, Y. Zhou, K. Liu, Z. Xiang, J. Ying, Z. Wang, T. Wu, X. Chen, Charge-density-wave-driven electronic nematicity in a kagome superconductor, *Nature* 604 (7904) (2022) 59–64. <https://doi.org/10.1038/s41586-022-04493-8>
- [56] Y. Sur, K.-T. Kim, S. Kim, K. H. Kim, Optimized superconductivity in the vicinity of a nematic quantum critical point in the kagome superconductor $\text{Cs}(\text{V}_{1-x}\text{Ti}_x)_3\text{Sb}_5$, *Nat. Commun.* 14 (1) (2023) 3899. <https://doi.org/10.1038/s41467-023-39495-1>
- [57] K. Chen, N. Wang, Q. Yin, Y. Gu, K. Jiang, Z. Tu, C. Gong, Y. Uwatoko, J. Sun, H. Lei, et al., Double superconducting dome and triple enhancement of T_c in the kagome superconductor CsV_3Sb_5 under high pressure, *Phys. Rev. Lett.* 126 (24) (2021) 247001. <https://link.aps.org/doi/10.1103/PhysRevLett.126.247001>
- [58] F. H. Yu, D. H. Ma, W. Z. Zhuo, S. Q. Liu, X. K. Wen, B. Lei, J. J. Ying, X. H. Chen, Unusual competition of superconductivity and charge-density-wave state in a compressed topological kagome metal, *Nature Communications* 12 (1) (2021) 3645. <https://doi.org/10.1038/s41467-021-23928-w>
- [59] L. Zheng, Z. Wu, Y. Yang, L. Nie, M. Shan, K. Sun, D. Song, F. Yu, J. Li, D. Zhao, S. Li, B. Kang, Y. Zhou, K. Liu, Z. Xiang, J. Ying, Z. Wang, T. Wu, X. Chen, Emergent charge order in pressurized kagome superconductor CsV_3Sb_5 , *Nature* 611 (7937) (2022) 682–687. <https://doi.org/10.1038/s41586-022-05351-3>
- [60] H. Tan, Y. Liu, Z. Wang, B. Yan, Charge density waves and electronic properties of superconducting kagome metals, *Phys. Rev. Lett.* 127 (4) (2021) 046401. <https://link.aps.org/doi/10.1103/PhysRevLett.127.046401>
- [61] H. Li, T. Zhang, T. Yilmaz, Y. Pai, C. Marvinney, A. Said, Q. Yin, C. Gong, Z. Tu, E. Vescovo, et al., Observation of unconventional charge density wave without acoustic phonon anomaly in kagome superconductors AV_3Sb_5 ($A = \text{Rb}, \text{Cs}$), *Phys. Rev. X* 11 (3) (2021) 031050. <https://link.aps.org/doi/10.1103/PhysRevX.11.031050>
- [62] A. Ptok, A. Kobialka, M. Sternik, J. Lazewski, P. T. Jochym, A. M. Oleś, P. Piekarczyk, Dynamical study of the origin of the charge density wave in AV_3Sb_5 ($A = \text{K}, \text{Rb}, \text{Cs}$) compounds, *Phys. Rev. B* 105 (2022) 235134. <https://link.aps.org/doi/10.1103/PhysRevB.105.235134>
- [63] C. Wang, S. Liu, H. Jeon, J.-H. Cho, Origin of charge density wave in the layered kagome metal CsV_3Sb_5 , *Phys. Rev. B* 105 (2022) 045135. <https://link.aps.org/doi/10.1103/PhysRevB.105.045135>
- [64] G. Liu, X. Ma, K. He, Q. Li, H. Tan, Y. Liu, J. Xu, W. Tang, K. Watanabe, T. Taniguchi, L. Gao, Y. Dai, H.-H. Wen, B. Yan, X. Xi, Observation of anomalous amplitude modes in the kagome metal CsV_3Sb_5 , *Nat Commun* 13 (1) (2022) 3461. <https://www.nature.com/articles/s41467-022-31162-1>
- [65] G. He, L. Peis, E. F. Cuddy, Z. Zhao, D. Li, Y. Zhang, R. Stumberger, B. Moritz, H. Yang, H. Gao, T. P. Devereaux, R. Hackl, Anharmonic strong-coupling effects at the origin of the charge density wave in CsV_3Sb_5 , *Nat Commun* 15 (1) (2024) 1895. <https://www.nature.com/articles/s41467-024-45865-0>
- [66] M. Gutierrez-Amigo, D. Dangić, C. Guo, C. Felser, P. J. Moll, M. G. Vergniory, I. Errea, Phonon collapse and anharmonic melting of the 3D charge-density wave in kagome metals, arXiv preprint arXiv:2311.14112 (2023). <https://arxiv.org/abs/2311.14112>
- [67] B. R. Ortiz, S. M. Teicher, L. Kautzsch, P. M. Sarte, N. Ratcliff, J. Harter, J. P. Ruff, R. Seshadri, S. D. Wilson, Fermi surface mapping and the nature of charge-density-wave order in the kagome superconductor CsV_3Sb_5 , *Phys. Rev. X* 11 (4) (2021) 041030. <https://link.aps.org/doi/10.1103/PhysRevX.11.041030>
- [68] Q. Stahl, D. Chen, T. Ritschel, C. Shekhar, E. Sadrolahi, M. Rahn, O. Ivashko, M. v. Zimmermann, C. Felser, J. Geck, Temperature-driven reorganization of electronic order in CsV_3Sb_5 , *Phys. Rev. B* 105 (19) (2022) 195136. <https://link.aps.org/doi/10.1103/PhysRevB.105.195136>
- [69] Q. Xiao, Y. Lin, Q. Li, X. Zheng, S. Francoual, C. Plueckthun, W. Xia, Q. Qiu, S. Zhang, Y. Guo, et al., Coexistence of multiple stacking charge density waves in kagome superconductor CsV_3Sb_5 , *Phys. Rev. Res.* 5 (1) (2023) L012032. <https://link.aps.org/doi/10.1103/PhysRevResearch.5.L012032>
- [70] L. Kautzsch, B. R. Ortiz, K. Mallayya, J. Plumb, G. Pokharel, J. P. Ruff, Z. Islam, E.-A. Kim, R. Seshadri, S. D. Wilson, Structural evolution of the kagome superconductors AV_3Sb_5 ($A = \text{K}, \text{Rb}, \text{and Cs}$) through charge density wave order, *Phys. Rev. Mater.* 7 (2) (2023) 024806. <https://link.aps.org/doi/10.1103/PhysRevMaterials.7.024806>
- [71] R. Markiewicz, A survey of the van hove scenario for high- T_c superconductivity with special emphasis on pseudogaps and striped phases, *Journal of Physics and Chemistry of Solids* 58 (8) (1997) 1179–1310.
- [72] K. Kim, S. Kim, J. S. Kim, H. Kim, J.-H. Park, B. I. Min, Importance of the van hove singularity in superconducting pdte_2 , *Phys. Rev. B* 97 (2018) 165102. doi:10.1103/PhysRevB.97.165102. <https://link.aps.org/doi/10.1103/PhysRevB.97.165102>
- [73] W. Wan, R. Harsh, P. Dreher, F. de Juan, M. M. Ugeda, Superconducting dome by tuning through a van hove singularity in a two-dimensional metal, *npj 2D Materials and Applications* 7 (2023) 41. doi:10.1038/s41699-023-00401-4. <http://dx.doi.org/10.1038/s41699-023-00401-4>
- [74] V. Y. Irkhin, A. A. Katanin, M. I. Katsnelson, Effects of van hove singularities on magnetism and superconductivity in the $t - t'$ hubbard model: A parquet approach, *Phys. Rev. B* 64 (2001) 165107. doi:10.1103/PhysRevB.64.165107. <https://link.aps.org/doi/10.1103/PhysRevB.64.165107>
- [75] I. I. Mazin, D. J. Singh, Electronic structure and magnetism in ru-based perovskites, *Phys. Rev. B* 56 (1997) 2556–2571. doi:10.1103/PhysRevB.56.2556. <https://link.aps.org/doi/10.1103/PhysRevB.56.2556>
- [76] H. Yamase, V. Oganesyan, W. Metzner, Mean-field theory for symmetry-breaking fermi surface deformations on a square lattice, *Phys. Rev. B* 72 (2005) 035114. doi:10.1103/PhysRevB.72.035114. <https://link.aps.org/doi/10.1103/PhysRevB.72.035114>
- [77] G. Kresse, J. Hafner, Ab initio molecular dynamics for liquid metals, *Phys. Rev. B* 47 (1993) 558–561. <https://link.aps.org/doi/10.1103/PhysRevB.47.558>
- [78] G. Kresse, J. Furthmüller, Efficiency of ab-initio total energy calculations for metals and semiconductors using a plane-wave basis set, *Computer. Mater. Sci.* 6 (1) (1996) 15–50. <http://www.sciencedirect.com/science/article/pii/S0927025696000080>
- [79] G. Kresse, J. Furthmüller, Efficient iterative schemes for ab initio total-energy calculations using a plane-wave basis set, *Phys. Rev. B* 54 (16) (1996) 11169. <https://link.aps.org/doi/10.1103/PhysRevB.54.11169>
- [80] G. Kresse, D. Joubert, From ultrasoft pseudopotentials to the projector augmented-wave method, *Phys. Rev. B* 59 (1999) 1758–1775. <https://link.aps.org/doi/10.1103/PhysRevB.59.1758>

- [81] J. P. Perdew, K. Burke, M. Ernzerhof, Generalized gradient approximation made simple, *Phys. Rev. Lett.* 77 (18) (1996) 3865.
<https://link.aps.org/doi/10.1103/PhysRevLett.77.3865>
- [82] P. E. Blöchl, Projector augmented-wave method, *Phys. Rev. B* 50 (24) (1994) 17953.
<https://link.aps.org/doi/10.1103/PhysRevB.50.17953>
- [83] S. Grimme, J. Antony, S. Ehrlich, H. Krieg, A consistent and accurate ab initio parametrization of density functional dispersion correction (DFT-D) for the 94 elements H-Pu, *J. Chem. Phys.* 132 (15) (2010) 154104.
<https://doi.org/10.1063/1.3382344>
- [84] G. Pizzi, V. Vitale, R. Arita, S. Blügel, F. Freimuth, G. Géranton, M. Gibertini, D. Gresch, C. Johnson, T. Kotrsune, J. Ibañez-Azpiroz, H. Lee, J.-M. Lihm, D. Marchand, A. Marrazzo, Y. Mokrousov, J. I. Mustafa, Y. Nohara, Y. Nomura, L. Paulatto, S. Poncé, T. Ponweiser, J. Qiao, F. Thöle, S. S. Tsirkin, M. Wierzbowska, N. Marzari, D. Vanderbilt, I. Souza, A. A. Mostofi, J. R. Yates, Wannier90 as a community code: new features and applications, *J. Phys. Condens. Matter* 32 (16) (2020) 165902.
<https://dx.doi.org/10.1088/1361-648X/ab51ff>
- [85] N. Marzari, D. Vanderbilt, Maximally localized generalized wannier functions for composite energy bands, *Phys. Rev. B* 56 (1997) 12847–12865.
<https://link.aps.org/doi/10.1103/PhysRevB.56.12847>
- [86] I. Souza, N. Marzari, D. Vanderbilt, Maximally localized wannier functions for entangled energy bands, *Phys. Rev. B* 65 (2001) 035109.
<https://link.aps.org/doi/10.1103/PhysRevB.65.035109>
- [87] N. Marzari, A. A. Mostofi, J. R. Yates, I. Souza, D. Vanderbilt, Maximally localized wannier functions: Theory and applications, *Rev. Mod. Phys.* 84 (2012) 1419–1475.
<https://link.aps.org/doi/10.1103/RevModPhys.84.1419>
- [88] M. Kawamura, Fermisurfer: Fermi-surface viewer providing multiple representation schemes, *Comput. Phys. Commun.* 239 (2019) 197–203.
<https://www.sciencedirect.com/science/article/pii/S0010465519300347>
- [89] M. Y. Jeong, H.-J. Yang, H. S. Kim, Y. B. Kim, S. Lee, M. J. Han, Crucial role of out-of-plane $sb\ p$ orbitals in van hove singularity formation and electronic correlations in the superconducting kagome metal CsV_3Sb_5 , *Phys. Rev. B* 105 (2022) 235145.
<https://link.aps.org/doi/10.1103/PhysRevB.105.235145>
- [90] H. Li, X. Liu, Y. B. Kim, H.-Y. Kee, Origin of π -shifted three-dimensional charge density waves in kagome metal AV_3Sb_5 , *Phys. Rev. B* 108 (2023) 075102.
<https://link.aps.org/doi/10.1103/PhysRevB.108.075102>
- [91] J. Deng, R. Zhang, Y. Xie, X. Wu, Z. Wang, Two elementary band representation model, fermi surface nesting, and surface topological superconductivity in AV_3Sb_5 ($A = K, Rb, Cs$), *Phys. Rev. B* 108 (2023) 115123.
<https://link.aps.org/doi/10.1103/PhysRevB.108.115123>
- [92] A. Subedi, Hexagonal-to-base-centered-orthorhombic 4Q charge density wave order in kagome metals KV_3Sb_5 , RbV_3Sb_5 , CsV_3Sb_5 , *Phys. Rev. Materials* 6 (1) (2022) 015001.
<https://link.aps.org/doi/10.1103/PhysRevMaterials.6.015001>
- [93] H. Yao, F. Yang, Topological odd-parity superconductivity at type-II two-dimensional van hove singularities, *Phys. Rev. B* 92 (2015) 035132.
<https://link.aps.org/doi/10.1103/PhysRevB.92.035132>
- [94] N. F. Q. Yuan, H. Isobe, L. Fu, Magic of high-order van hove singularity, *Nat. Commun.* 10 (1) (Dec. 2019).
<http://dx.doi.org/10.1038/s41467-019-13670-9>
- [95] L. Classen, J. J. Betouras, High-order Van Hove singularities and their connection to flat bands, arXiv preprint arXiv:2405.20226 (2024).
<https://arxiv.org/abs/2405.20226>
- [96] Y. Hu, X. Wu, B. R. Ortiz, X. Han, N. C. Plumb, S. D. Wilson, A. P. Schnyder, M. Shi, et al., Coexistence of trihexagonal and star-of-david pattern in the charge density wave of the kagome superconductor AV_3Sb_5 , *Phys. Rev. B* 106 (24) (2022) L241106.
<https://link.aps.org/doi/10.1103/PhysRevB.106.L241106>
- [97] S. Sim, M. Y. Jeong, H. Lee, D. H. D. Lee, M. J. Han, Chemical effect on the van hove singularity in superconducting kagome metal AV_3Sb_5 ($A = K, Rb, \text{ and } Cs$), *Physical Chemistry Chemical Physics* 26 (15) (2024) 11715–11721.
<http://dx.doi.org/10.1039/D4CP00517A>

Supplemental Information for
“Stacking-Dependent Van Hove Singularity Shifts in
Three-Dimensional Charge Density Waves of Kagome Metals
 AV_3Sb_5 ($A = K, Rb, Cs$)”

Chanchal K. Barman^{1,*}, Sun-Woo Kim^{2,*}, Youngkuk Kim^{1,†}

¹ *Department of Physics, Sungkyunkwan University, Suwon 16419, Korea*

² *Department of Materials Science and Metallurgy, University of Cambridge, 27 Charles
Babbage Road, Cambridge, United Kingdom*

Contents

Tight-binding Hamiltonian	2
Dispersion near the type-II van Hove singularities from TB Hamiltonian	6

TIGHT-BINDING HAMILTONIAN

In this section, we provide a detailed description of each matrix term in our tight-binding (TB) Hamiltonian. Schematic representations of the nearest neighbor (NN), next-nearest neighbor (NNN) hopping within the 2D kagome layer, and interlayer hopping between the vertically stacked kagome layers are illustrated in Fig. S1. Considering a basis set $\Psi_k^T = (A_k^T, B_k^T, C_k^T)$ and $\alpha_k^T = (\alpha_{1,k}, \alpha_{2,k}, \alpha_{3,k}, \alpha_{4,k})$, where α_i represents sublattice index for vanadium sites in the 2×2 unit cell as shown in Fig. S1, we express the hopping matrices as follows:

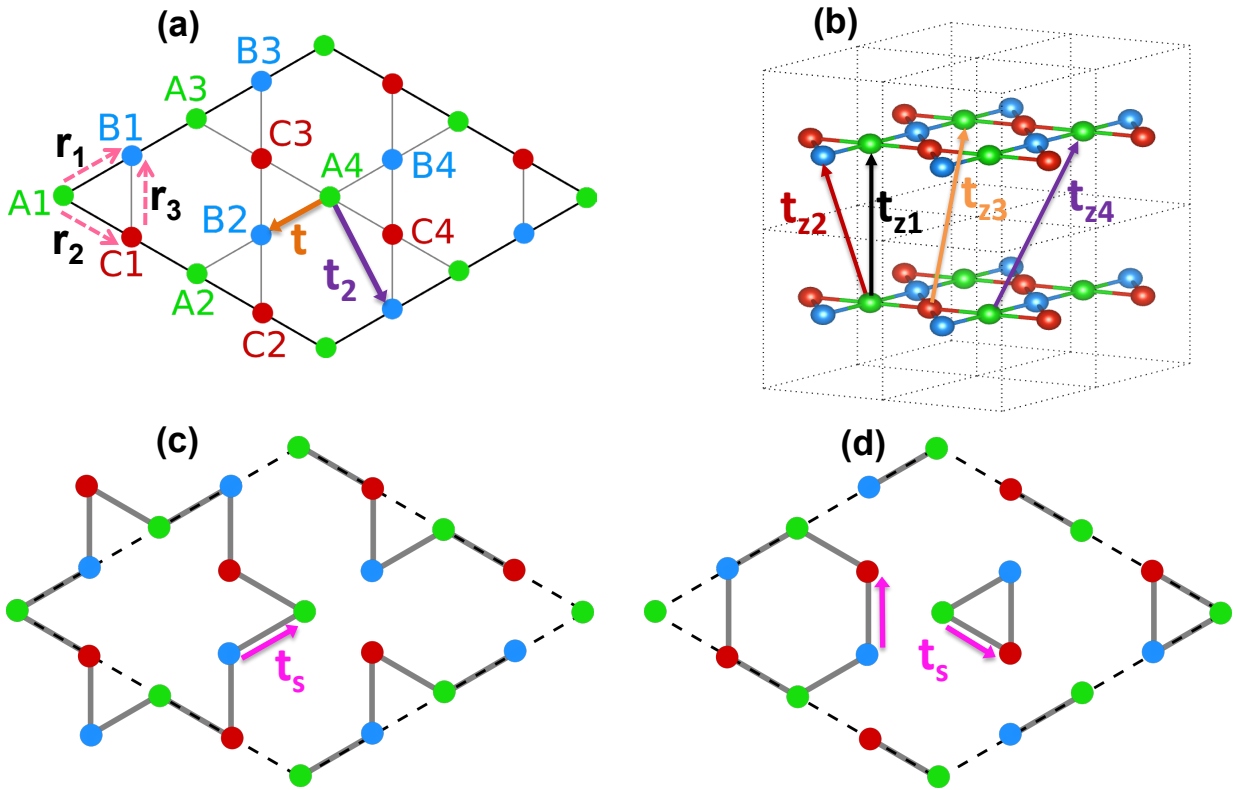


FIG. S1: (Color online) (a) 2×2 unit cell with sublattice indices. t and t_2 are NN and NNN hopping strength. (b) Kagome layers stacked along z -direction. t_{z1} , t_{z2} , t_{z3} , and t_{z4} are NN, NNN, NNNN, and NNNNN hopping strengths along z -direction. (c,d) CDW structure with SD and ISD distortion.

$$\mathcal{H}_{NN}(\mathbf{k}) = -t \begin{pmatrix} \varepsilon & 0 & 0 & 0 & \phi_1 & 0 & \phi_1^* & 0 & \phi_2 & \phi_2^* & 0 & 0 \\ \varepsilon & 0 & 0 & 0 & \phi_1 & 0 & \phi_1^* & \phi_2^* & \phi_2 & 0 & 0 & 0 \\ \varepsilon & 0 & \phi_1^* & 0 & \phi_1 & 0 & 0 & 0 & 0 & \phi_2 & \phi_2^* & 0 \\ \varepsilon & 0 & \phi_1^* & 0 & \phi_1 & 0 & 0 & 0 & \phi_2^* & \phi_2 & 0 & 0 \\ \varepsilon & 0 & 0 & 0 & \phi_3^* & 0 & 0 & 0 & \phi_3 & 0 & 0 & 0 \\ \varepsilon & 0 & 0 & 0 & \phi_3^* & \phi_3 & 0 & 0 & 0 & 0 & 0 & 0 \\ \varepsilon & 0 & 0 & \phi_3 & \phi_3^* & 0 & 0 & 0 & 0 & 0 & 0 & 0 \\ h.c. & \varepsilon & \phi_3 & 0 & 0 & \phi_3^* & 0 & 0 & 0 & 0 & 0 & 0 \\ \varepsilon & 0 & 0 & 0 & 0 & 0 & 0 & 0 & 0 & 0 & 0 & 0 \\ \varepsilon & 0 & 0 & 0 & 0 & 0 & 0 & 0 & 0 & 0 & 0 & 0 \\ \varepsilon & 0 & 0 & 0 & 0 & 0 & 0 & 0 & 0 & 0 & 0 & 0 \\ \varepsilon & 0 & 0 & 0 & 0 & 0 & 0 & 0 & 0 & 0 & 0 & 0 \\ \varepsilon & 0 & 0 & 0 & 0 & 0 & 0 & 0 & 0 & 0 & 0 & 0 \\ \varepsilon & 0 & 0 & 0 & 0 & 0 & 0 & 0 & 0 & 0 & 0 & 0 \end{pmatrix} \quad (\text{S1})$$

$$\mathcal{H}_{NNN}(\mathbf{k}) = -t_2 \begin{pmatrix} 0 & 0 & 0 & 0 & 0 & \phi_6^* & 0 & \phi_6 & 0 & 0 & \phi_5^* & \phi_5 \\ 0 & 0 & 0 & \phi_6^* & 0 & \phi_6 & 0 & 0 & 0 & 0 & \phi_5 & \phi_5^* \\ 0 & 0 & 0 & \phi_6 & 0 & \phi_6^* & \phi_5^* & \phi_5 & 0 & 0 & 0 & 0 \\ 0 & \phi_6 & 0 & \phi_6^* & 0 & \phi_5 & \phi_5^* & 0 & 0 & 0 & 0 & 0 \\ 0 & 0 & 0 & 0 & 0 & 0 & \phi_4^* & \phi_4 & 0 & 0 & 0 & 0 \\ 0 & 0 & 0 & \phi_4^* & 0 & 0 & 0 & \phi_4 & 0 & 0 & 0 & 0 \\ 0 & 0 & \phi_4 & 0 & 0 & 0 & \phi_4^* & 0 & 0 & 0 & 0 & 0 \\ h.c. & 0 & 0 & \phi_4 & \phi_4^* & 0 & 0 & 0 & 0 & 0 & 0 & 0 \\ 0 & 0 & \phi_4 & \phi_4^* & 0 & 0 & 0 & 0 & 0 & 0 & 0 & 0 \\ 0 & 0 & 0 & 0 & 0 & 0 & 0 & 0 & 0 & 0 & 0 & 0 \\ 0 & 0 & 0 & 0 & 0 & 0 & 0 & 0 & 0 & 0 & 0 & 0 \\ 0 & 0 & 0 & 0 & 0 & 0 & 0 & 0 & 0 & 0 & 0 & 0 \\ 0 & 0 & 0 & 0 & 0 & 0 & 0 & 0 & 0 & 0 & 0 & 0 \end{pmatrix} \quad (\text{S2})$$

$$\mathcal{H}_{NN}^{3D}(\mathbf{k}) = -2t_{z1} \phi_z \mathbb{I}_{12} \quad (\text{S5})$$

$$\mathcal{H}_{N\bar{N}\bar{N}}^{3D}(\mathbf{k}) = -t_{z2} \phi_z \mathcal{H}_{NN}(\mathbf{k}) \quad (\text{S6})$$

$$\mathcal{H}_{\bar{N}\bar{N}\bar{N}\bar{N}}^{3D}(\mathbf{k}) = -t_{z3} \phi_z \mathcal{H}_{N\bar{N}\bar{N}}(\mathbf{k}) \quad (\text{S7})$$

$$\mathcal{H}_{\bar{N}\bar{N}\bar{N}\bar{N}\bar{N}}^{3D}(\mathbf{k}) = -t_{z4} \mathbb{I}_3 \otimes \Lambda \quad (\text{S8})$$

$$\Lambda = 2\phi_z \begin{pmatrix} 0 & \cos(\mathbf{k} \cdot \nu_9) & \cos(\mathbf{k} \cdot \nu_8) & \cos(\mathbf{k} \cdot \nu_7) \\ & 0 & \cos(\mathbf{k} \cdot \nu_7) & \cos(\mathbf{k} \cdot \nu_8) \\ h.c. & & 0 & \cos(\mathbf{k} \cdot \nu_9) \\ & & & 0 \end{pmatrix} \quad (\text{S9})$$

In the above, \mathbb{I}_3 and \mathbb{I}_{12} are 3×3 and 12×12 identity matrices respectively and ε is the onsite energy. The notations, $\phi_j = e^{i\mathbf{k} \cdot \mathbf{r}_j}$ for $j \in (1, 3)$ and $\phi_j = e^{i\mathbf{k} \cdot \nu_j}$ for $\nu \in (4, 6)$, $\phi_z = \cos(\mathbf{k} \cdot \mathbf{r}_z)$ and the position vectors are $\mathbf{r}_1 = \frac{1}{2}(\sqrt{3}, 1)$, $\mathbf{r}_2 = \frac{1}{2}(\sqrt{3}, -1)$, $\mathbf{r}_3 = (0, 1)$, $\nu_4 = \mathbf{r}_1 + \mathbf{r}_2$, $\nu_5 = \mathbf{r}_1 + \mathbf{r}_3$, $\nu_6 = \mathbf{r}_2 - \mathbf{r}_3$, $\nu_7 = 2\mathbf{r}_3$, $\nu_8 = 2\mathbf{r}_1$, $\nu_9 = 2\mathbf{r}_3$, $\mathbf{r}_z = (0, 0, c_z)$. Here, $c_z = 1.643, 1.680, 1.715$ for KV_3Sb_5 , RbV_3Sb_5 , and CsV_3Sb_5 respectively.

DISPERSION NEAR THE TYPE-II VAN HOVE SINGULARITIES FROM TB HAMILTONIAN

In this section, using the TB Hamiltonian we present an effective low-energy expansion of the dispersion around the vicinity of the type-II VHSs, as illustrated in Fig. 2 of the main manuscript. The expression for the dispersion polynomial is detailed in Eq. (S10). k_x and k_y are crystal momenta relative to the VHS point. Details about the various parameters in the dispersion are listed in Table S1.

$$E_k = \varepsilon_0 + \alpha k_y + \beta_1 k_x^2 + \beta_2 k_y^2 + \gamma_1 k_y^3 + \gamma_2 k_x^2 k_y + \delta_1 k_x^4 + \delta_2 k_y^4 + \delta_3 k_x^2 k_y^2 \quad (\text{S10})$$

TABLE S1: Various parameters of the dispersion in Eq. (S10). The unit of ε_0 , α , β_i , γ_i and δ_i are given in eV, eV.Å, eV.Å², eV.Å³, and eV.Å⁴ respectively.

	ε_0	α	β_1	β_2	γ_1	γ_2	δ_1	δ_2	δ_3
CsV ₃ Sb ₅	-0.0346	0.0001	0.1949	-0.4190	0.9303	-0.7292	-2.3940	0.5209	5.3077
KV ₃ Sb ₅	-0.0069	-0.0068	0.6582	-0.6517	0.3313	-2.0620	-5.5080	2.1522	2.7612
RbV ₃ Sb ₅	-0.0288	0.0107	0.5389	-0.6531	0.4393	-1.8213	-4.3305	1.9734	4.3466